Available online at www.sciencedirect.com
SCIENCE DIRECT®
Journal of Sound and Vibration 291 (2006) 779–801
JOURNAL OF SOUND AND VIBRATION
www.elsevier.com/locate/jsvi

Effect of mean entropy on unsteady disturbance propagation in a slowly varying duct with mean swirling flow

A.J. Cooper*

School of Engineering, University of Warwick, Gibbet Hill Road, Coventry, CV4 7AL, UK

Received 25 June 2004; received in revised form 12 April 2005; accepted 27 June 2005
Available online 2 November 2005

Abstract

The propagation of acoustic disturbances in a slowly-varying duct with mean swirling flow and non-uniform mean entropy is considered. This is representative of the region of swirling flow downstream of the rotor in aeroengine applications where variations in mean entropy can be significant. The duct is assumed to vary slowly in axial cross section and a consistent multiple-scales solution is derived. The variation in axial wavenumber and amplitude of the duct modes is determined as part of the solution.

Comparisons are made between the cases of isentropic and non-isentropic flow. The cut-on/cut-off characteristics of a given mode are altered by any form of non-uniform mean entropy, with modes pushed closer to cut-off resulting in larger variations in amplitude. The greatest departure from the baseline isentropic result occurs for a positive entropy gradient. Increasing the swirl velocity at the duct inlet leads to increasing levels of mean entropy.

1. Introduction

The way in which acoustic disturbances propagate through sections of an aeroengine is crucial for understanding and predicting the generation of noise and instabilities within the engine. The geometry of the aeroengine duct and the region of mean swirling flow downstream of the rotor have a significant impact on both of these phenomena. The propagation of unsteady disturbances

*Tel.: +44 24 765 23086; fax: +44 24 764 18922.
E-mail address: a.j.cooper@warwick.ac.uk.

0022-460X/$ - see front matter © 2005 Elsevier Ltd. All rights reserved.
doi:10.1016/j.jsv.2005.06.041

in a slowly-varying duct with mean swirling flow was addressed by Cooper and Peake [1]. This analysis was carried out under the assumptions of isentropic flow and no entropic disturbance generation. However in turbomachinery applications, variations in mean entropy can be significant. The aim of this paper, therefore, is to address what effect different mean entropy distributions have on the propagation of disturbances in mean swirling flow in a duct which varies slowly in axial cross section.

There is natural interest in sound transmission through ducts of varying cross section since in practical applications it is likely that ducts will not be exactly uniform. The problem of a circular duct with varying cross section carrying irrotational flow was considered by Nayfeh and co-workers [2–4], and more recently by Rienstra [5] who developed a consistent multiple-scales solution based on the assumption of a slow axial scale $X = \varepsilon x$, where ε is a small parameter related to the axial slope of the duct walls and x is the standard axial coordinate. This method was compared very successfully with a fully numerical solution by Rienstra and Eversman [6]. The consistent multiple-scales approach was extended by Peake and Cooper [7] to consider acoustic propagation in ducts with slowly-varying elliptic cross section. This was then followed by a generalized solution for acoustic propagation in ducts of arbitrary cross section by Rienstra [8]. Cooper and Peake [1] derived a multiple-scales solution for a slowly-varying circular duct where there exists non-zero mean vorticity. The analysis for ducts carrying mean vortical flow is more complicated than the one for irrotational flow since the acoustic and vorticity equations become coupled and the system of equations is not self-adjoint.

Little work has been carried out on the effects of mean entropy gradient in mean swirling flows even for the case of uniform ducts. For homentropic flow in a uniform duct Golubev and Atassi [9] showed that unsteady disturbances have both a potential and vortical part and as a result the solutions to the governing equations are coupled acoustic–vorticity waves. Two distinct families of solutions exist; one which is pressure-dominated, analogous to acoustic waves in irrotational flow and well-defined by a modal decomposition, and a second which is vorticity-dominated. Golubev and Atassi [9] showed that for the vorticity-dominated waves a critical layer exists in the eigenmode spectrum and as such it is not generally appropriate to describe these vortical waves in terms of modes, but instead as the solution to an initial-value problem [10]. Under the assumption of non-isentropic flow the energy equation is also coupled to the acoustic and vorticity equations, and the solution must be expressed in terms of potential, vortical and entropic components. The two distinct families of eigensolutions are still found to exist. This paper is concerned with sound propagation and attention is therefore restricted to the pressure-dominated waves. The analysis of Tam and Auriault [11] assumed, indirectly, a mean flow with non-zero mean entropy through the assumption of uniform mean density. However, the governing equations for the disturbance did not account for any entropic disturbances. Entropy generation has been investigated for swirling jets impinging onto an adiabatic wall [12,13], where it was found that increasing the swirl velocity enhanced the entropy generation.

In this paper a multiple-scales analysis, based on the techniques used by Rienstra [5] and Cooper and Peake [1], is carried out on the coupled system of acoustic, vorticity and energy equations. The general problem is set out in Section 2. In Section 3 the steady mean flow solution is determined in terms of a steady streamfunction and calculated as a numerical solution, given a prescribed set of initial conditions. In Section 4 the $O(1)$ approximation to the unsteady flow is determined by solving an eigenvalue problem at each axial location. The variation of the axial

wavenumber along the duct is calculated at this order which determines which modes are cut-on (propagate) or cut-off (evanescent). The equations which determine the $O(\varepsilon)$ correction to the unsteady flow are used to define a governing equation for the amplitude variation of the leading-order solution. In Section 5 the results based on two sets of initial conditions are presented. Firstly, in order to determine the effects of mean entropy on the propagation of disturbances, different initial mean entropy distributions are prescribed at the duct inlet. It is shown that both the cut-on/cut-off behaviour of the modes and the variation in amplitude are affected significantly by the form of the mean entropy distribution. Secondly uniform mean density is prescribed at the inlet, together with different swirl distributions. The level of mean swirl is found to affect the level of mean entropy generated, as well as the characteristics of the disturbance propagation.

2. Problem formulation

Consider a cylindrical duct, with coordinate system (x, r, θ), which varies slowly in axial cross section and contains a compressible, inviscid, polytropic gas. Lengths are non-dimensionalized by a reference duct radius, R_∞, velocities on a reference sound speed, c_∞, density by ρ_∞ and pressure by $\rho_\infty c_\infty^2$, and all quantities used subsequently are non-dimensional.

The duct is defined in terms of a slow axial scale $X = \varepsilon x$, where ε is a small parameter which characterizes the slope of the duct walls, such that

$$0 \leqslant R_1(X) \leqslant r \leqslant R_2(X). \tag{1}$$

The parameter ε is used as an asymptotic parameter to determine a consistent multiple-scales solution. The general flow is described in terms of the velocity field $\mathbf{v}$, sound speed c, density ρ, pressure p and entropy s. The fluid motion is governed by the equations for conservation of mass, momentum and energy

$$\frac{\partial \rho}{\partial t} + \nabla \cdot (\rho \mathbf{v}) = 0, \tag{2}$$

$$\rho\left(\frac{\partial \mathbf{v}}{\partial t} + \mathbf{v} \cdot \nabla \mathbf{v}\right) = -\nabla p, \tag{3}$$

$$\frac{\partial s}{\partial t} + \mathbf{v} \cdot \nabla s = 0, \tag{4}$$

together with the relations

$$\frac{\rho^\gamma}{\gamma p} = \mathrm{e}^{-s/c_v}, \quad c^2 = \frac{\gamma p}{\rho}, \tag{5}$$

where $\gamma = c_p/c_v$ is a gas constant, c_v is the specific heat capacity at constant volume and c_p is the specific heat capacity at constant pressure, both taken to be constant. Note that if s_∞ is the reference entropy value then $\gamma = \exp(s_\infty/c_v)$. The state $s = 0$ then reduces the problem to that obtained by standard isentropic flow assumptions (see Ref. [1] for rotational flow and Ref. [5] in the limit of zero mean vorticity).

The total flow field is assumed to be composed of an axisymmetric steady mean flow and a small unsteady perturbation such that

$$[\mathbf{v}, c, \rho, p, s](x, r, \theta, t) = [\mathbf{V}, C, D, P, S](X, r) + [\tilde{\mathbf{v}}, \tilde{c}, \tilde{\rho}, \tilde{p}, \tilde{s}](x, r, \theta, t). \tag{6}$$

3. Mean flow

Assuming the flow field takes the form in Eq. (6) the governing equations (2)–(4) are linearized to yield the following equations which govern the mean flow:

$$\nabla \cdot (D\mathbf{V}) = 0, \tag{7}$$

$$D\mathbf{V} \cdot \nabla \mathbf{V} = -\nabla P, \tag{8}$$

$$\mathbf{V} \cdot \nabla S = 0. \tag{9}$$

If the mean velocity field is of the form

$$\mathbf{V} = U(X, r; \varepsilon)\mathbf{e}_x + V(X, r; \varepsilon)\mathbf{e}_r + W(X, r; \varepsilon)\mathbf{e}_\theta, \tag{10}$$

then with

$$\frac{\partial}{\partial x} = \varepsilon \frac{\partial}{\partial X}, \tag{11}$$

the steady continuity equation (7) shows that $O(\varepsilon)$ axial variations must be balanced by $O(\varepsilon)$ radial variations. This leads to the following expansions in terms of the asymptotic parameter ε:

$$[U, W, C, D, P, S](X, r; \varepsilon) = [U_0, W_0, C_0, D_0, P_0, S_0](X, r) + O(\varepsilon^2), \tag{12}$$

$$V(X, r; \varepsilon) = \varepsilon V_1(X, r) + O(\varepsilon^3). \tag{13}$$

The calculation of the mean flow field is based on the analysis given in Section 7.5 of Ref. [14] for incompressible flow in a variable-area pipe. This was modified in Ref. [1] to include compressibility and is further modified here to include non-zero mean entropy.

The mean vorticity, $\boldsymbol{\xi}$, for the velocity field in Eqs. (12) and (13) is

$$\boldsymbol{\xi} = \frac{1}{r}\frac{\partial (rW_0)}{\partial r}\mathbf{e}_x - \varepsilon \frac{\partial W_0}{\partial X}\mathbf{e}_r - \frac{\partial U_0}{\partial r}\mathbf{e}_\theta + O(\varepsilon^2). \tag{14}$$

The continuity equation (7) can be satisfied by writing the velocity components U_0 and V_1 in terms of a streamfunction, $\psi(X, r)$, such that

$$U_0 = \frac{1}{rD_0}\frac{\partial \psi}{\partial r}, \quad V_1 = -\frac{1}{rD_0}\frac{\partial \psi}{\partial X}. \tag{15}$$

Using Bernoulli's equation, the θ-momentum equation, and the entropy equation, the enthalpy (H) the circulation (C) and the mean entropy ($\mathscr{S}$) can be written as arbitrary functions of ψ

$$\frac{1}{2}(U_0^2 + W_0^2) + \frac{D_0^{\gamma-1}\mathrm{e}^{S_0/c_v}}{\gamma - 1} = H(\psi), \tag{16}$$

$$rW_0 = C(\psi), \tag{17}$$

$$S_0 = \mathscr{S}(\psi). \tag{18}$$

Eqs. (17) and (18) state that the circulation and mean entropy are constant along a streamline. For non-isentropic flow Crocco's relation,

$$\mathbf{V} \times \boldsymbol{\xi} = \nabla H - T\nabla\mathscr{S}, \tag{19}$$

where $T = P_0/(RD_0)$ is the temperature ($R = c_p - c_v$), which can be used to obtain an expression for the azimuthal vorticity, ξ_θ, in terms of H, C and $\mathscr{S}$. Taking the r-component of Eq. (19) leads to the identity

$$W_0\xi_x - U_0\xi_\theta = \frac{\partial H}{\partial r} - T\frac{\partial \mathscr{S}}{\partial r} = rD_0U_0[H'(\psi) - T\mathscr{S}'(\psi)], \tag{20}$$

where $'$ denotes differentiation with respect to ψ. Substituting for ξ_x from Eq. (14) and using Eq. (17) gives

$$\xi_\theta = W_0D_0C'(\psi) - rD_0[H'(\psi) - T\mathscr{S}'(\psi)]. \tag{21}$$

Using the expression for ξ_θ in Eq. (14) the following equation governing ψ and D_0 is obtained:

$$\frac{\partial}{\partial r}\left(\frac{1}{rD_0}\frac{\partial\psi}{\partial r}\right) = rD_0[H'(\psi) - T\mathscr{S}'(\psi)] - D_0C'(\psi)\frac{C}{r}. \tag{22}$$

Writing the Bernoulli condition (16) in terms of ψ and D_0 gives a second equation governing the evolution of ψ and D_0:

$$\frac{1}{2}\frac{1}{r^2D_0^2}\left(\frac{\partial\psi}{\partial r}\right)^2 + \frac{C^2}{2r^2} + \frac{D_0^{\gamma-1}e^{\mathscr{S}/c_v}}{\gamma - 1} = H(\psi). \tag{23}$$

The associated boundary conditions which, together with Eqs. (22) and (23), govern the mean flow field are

$$\psi(X, r = R_1) = 0, \quad \psi(X, r = R_2) = \text{constant}. \tag{24}$$

For a hollow duct the first condition is replaced by $\psi \propto r^2$ as $r \to 0$. The constant in Eq. (24) is determined from initial conditions specified at the inlet of the duct. Note that the dependence on X occurs only through the variation in the boundary condition.

Eqs. (22) and (23) can be solved numerically for any set of inlet conditions. Here two cases are analysed which enable the functions H, C and $\mathscr{S}$ to be determined analytically. Under standard isentropic flow assumptions only initial conditions for the velocity components need be prescribed since the initial density can be obtained from the radial momentum equation. For non-isentropic flow an additional condition must be prescribed. In the first case the initial mean entropy distribution is chosen as the additional prescribed inlet condition. The second case involves prescribing uniform density at the inlet. Results of the computations are given in Section 5.

4. Disturbance field

4.1. Governing equations

In order to determine the evolution of the unsteady disturbance field the unsteady, rotational, disturbance velocity is decomposed, following Goldstein [15] into potential, vortical and entropic components as follows:

$$\tilde{\mathbf{v}} = \nabla\phi + \mathbf{u}^R + \tilde{s}\mathbf{V}/2c_p. \tag{25}$$

The unsteady pressure is expressed solely in terms of the potential by

$$\tilde{p} = -D_0\frac{D\phi}{Dt}, \tag{26}$$

where $D/Dt \equiv (\partial/\partial t) + \mathbf{V}\cdot\nabla$ is the convective derivative. The linearized equations obtained from Eqs. (2)–(4) can then be written in the form

$$\frac{D}{Dt}\left(\frac{D_0}{C_0^2}\frac{D\phi}{Dt}\right) - \nabla(D_0\nabla\phi) = \nabla\cdot(D_0\mathbf{u}^R) + \mathbf{V}\cdot\nabla\left(\frac{D_0\tilde{s}}{2c_p}\right) - \frac{1}{c_p}\frac{D}{Dt}(D_0\tilde{s}) - \left(\frac{D_0}{C_0^2}\frac{D\phi}{Dt} + \frac{D_0\tilde{s}}{2c_p}\right)\nabla\cdot\mathbf{V}, \tag{27}$$

$$\frac{D\mathbf{u}^R}{Dt} + \mathbf{u}^R\cdot\nabla\mathbf{V} = \nabla\phi\times\boldsymbol{\xi} - \frac{D\phi}{Dt}\frac{\nabla S_0}{c_p} - \frac{\mathbf{V}}{2c_p}\frac{D\tilde{s}}{Dt}, \tag{28}$$

$$\frac{D\tilde{s}}{Dt} + \left(\nabla\phi + \mathbf{u}^R + \frac{\tilde{s}\mathbf{V}}{2c_p}\right)\cdot\nabla S_0 = 0. \tag{29}$$

The boundary conditions implemented allow for the inclusion of acoustic lining on the duct walls. The inner and outer duct walls are taken to have complex impedances Z_1 and Z_2, respectively, with hard wall boundary conditions given by the limit $Z_j \to \infty$. The boundary conditions for an arbitrary mean flow along a curved wall, defined originally by Myers [16] and implemented by Rienstra [5] and Cooper and Peake [1], are

$$-\mathrm{i}\omega(\tilde{\mathbf{v}}\cdot\mathbf{n}_j) = [-\mathrm{i}\omega + \mathbf{V}\cdot\nabla - \mathbf{n}_j\cdot(\mathbf{n}_j\cdot\nabla\mathbf{V})]\left(\frac{\tilde{p}}{Z_j}\right) \quad \text{at } r = R_j(X), \quad j = 1, 2, \tag{30}$$

where $\mathbf{n}_j$ are the outward-directed normal vectors at the wall.

4.2. Leading-order solution

For the acoustic modes found in mean swirling flow the method of multiple scales is used to obtain the perturbation solution. The solution is assumed to have a slowly-varying amplitude

with a phase variation of the form

$$(\phi, u_x^R, u_r^R, u_\theta^R, \tilde{s}/c_p)(x,r,\theta,t;\varepsilon) = [(A_0, \mathscr{X}_0, \mathscr{R}_0, \mathscr{T}_0, \hat{s}_0)(X,r;\varepsilon) + \varepsilon(A_1, \mathscr{X}_1, \mathscr{R}_1, \mathscr{T}_1, \hat{s}_1)(X,r;\varepsilon) + O(\varepsilon^2)] \exp\left(\frac{\mathrm{i}}{\varepsilon}\int^X k(\eta)\,\mathrm{d}\eta + \mathrm{i}m\theta - \mathrm{i}\omega t\right), \tag{31}$$

where k is the axial wavenumber, m the circumferential wavenumber and ω the frequency. The unknown axial wavenumber and amplitudes are determined as part of the solution. (Note that for the vortical disturbances not considered here the amplitudes would depend on both x and X.) Substitution of the disturbance form in Eq. (31) into the governing equations (27)–(29) and taking $O(1)$ terms gives

$$\frac{\partial^2 A_0}{\partial r^2} + \left(\frac{1}{r} + \frac{\partial \ln D_0}{\partial r}\right)\frac{\partial A_0}{\partial r} + \left(\frac{\Lambda^2}{C_0^2} - \frac{m^2}{r^2} - k^2\right)A_0 + \frac{\partial \mathscr{R}_0}{\partial r} + \left(\frac{1}{r} + \frac{\partial \ln D_0}{\partial r}\right)\mathscr{R}_0 + \frac{\mathrm{i}m\mathscr{T}_0}{r} + \mathrm{i}k\mathscr{X}_0 + (\omega - \Lambda)\frac{\mathrm{i}\hat{s}_0}{2} = 0, \tag{32}$$

$$\mathrm{i}\Lambda\mathscr{X}_0 + \frac{\partial U_0}{\partial r}\left(\frac{\partial A_0}{\partial r} + \mathscr{R}_0\right) + \frac{U_0}{2}\mathrm{i}\Lambda\hat{s}_0 = 0, \tag{33}$$

$$\mathrm{i}\Lambda\mathscr{R}_0 - \frac{2W_0\mathscr{T}_0}{r} - \frac{\Gamma \mathrm{i}mA_0}{r} - \frac{\partial U_0}{\partial r}\mathrm{i}kA_0 + \frac{\mathrm{i}\Lambda A_0}{\gamma}\frac{\partial \hat{S}_0}{\partial r} = 0, \tag{34}$$

$$\mathrm{i}\Lambda\mathscr{T}_0 + \Gamma\left(\frac{\partial A_0}{\partial r} + \mathscr{R}_0\right) + \frac{W_0}{2}\mathrm{i}\Lambda\hat{s}_0 = 0, \tag{35}$$

$$\mathrm{i}\Lambda\hat{s}_0 + \left(\frac{\partial A_0}{\partial r} + \mathscr{R}_0\right)\frac{1}{\gamma}\frac{\partial \hat{S}_0}{\partial r} = 0, \tag{36}$$

where $\hat{S}_0 = S_0/c_v$, $\Gamma = (1/r)\partial(rW_0)/\partial r$ and $\Lambda = kU_0 - \omega + mW_0/r$. The $O(1)$ terms in the boundary condition (30) are

$$\mathrm{i}\omega\left(\frac{\partial A_0}{\partial r} + \mathscr{R}_0\right) \mp \frac{D_0\Lambda^2 A_0}{Z_j} = 0, \tag{37}$$

where $\mp$ refers to evaluation at $R_1(X)$ and $R_2(X)$, respectively.

Comparing Eqs. (33) and (35) gives

$$\mathscr{X}_0 = \frac{\partial U_0}{\partial r}\frac{\mathscr{T}_0}{\Gamma} - \left(U_0 - \frac{\partial U_0}{\partial r}\frac{W_0}{\Gamma}\right)\frac{\hat{s}_0}{2}. \tag{38}$$

Following the elimination of Eq. (33), the remaining Eqs. (32) and (34)–(36) can be expressed in the form of a linear eigenvalue problem

$$(\mathscr{L} - k\mathscr{K})\boldsymbol{\psi}_0 \equiv \mathscr{F}\boldsymbol{\psi}_0 = 0, \tag{39}$$

where $\boldsymbol{\psi}_0 = (A_0, \eta_0, \mathscr{R}_0, \mathrm{i}\mathscr{T}_0, \mathrm{i}\hat{s}_0)$, with $\eta_0 = k\beta_0^2 A_0$ and $\beta_0^2 = 1 - U_0^2/C_0^2$. The operators $\mathscr{L}$ and $\mathscr{K}$ are defined in Appendix A.

The $O(1)$ linear eigenvalue problem in Eq. (39), together with the boundary conditions in Eq. (37), is solved numerically using a Chebyshev spectral collocation method with a staggered grid as described by Khorrami [17]. The eigenvalue problem is solved at each axial location to determine the axial wavenumber $k(X)$ and a normalized numerical eigenfunction $\hat{\boldsymbol{\psi}}_0(X,r)$. The leading-order unsteady solution is then given by

$$\boldsymbol{\psi}_0(X,r) = N(X)\hat{\boldsymbol{\psi}}_0(X,r), \tag{40}$$

where $N(X)$ is an arbitrary function which is determined from the fact that the $O(\varepsilon)$ problem is solvable. Any solvability condition which gives ψ_0 without having to determine ψ_1 can be applied. Here the approach based on the adjoint operator is used [5,1]. The solvability condition and the solution for $N(X)$ is described in the next section.

4.3. First-order solution

The $O(\varepsilon)$ terms in the governing equations for the unsteady flow can be written in the form

$$(\mathscr{L} - k\mathscr{K})\boldsymbol{\psi}_1 \equiv \mathscr{F}\boldsymbol{\psi}_1 = \mathbf{f}, \tag{41}$$

where $\mathbf{f}$ is defined in Appendix B and $\boldsymbol{\psi}_1 = (A_1, \eta_1, \mathscr{R}_1, \mathrm{i}\mathscr{T}_1, \mathrm{i}\hat{s}_1)$, with $\eta_1 = k\beta_0^2 A_1$. The corresponding $O(\varepsilon)$ boundary conditions are

$$\begin{aligned}\mathrm{i}\omega\left(\frac{\partial A_1}{\partial r} + \mathscr{R}_1\right) \mp \frac{D_0 \Lambda^2 A_1}{Z_j} = {} & \mathrm{i}\omega\frac{\partial R_j}{\partial X}(\mathrm{i}kA_0 + \mathscr{X}_0 + U_0\hat{s}_0/2) - \frac{\mathrm{i}\omega V_1 \hat{s}_0}{2} \\ & \mp \frac{\mathrm{i}}{A_0}\left[U_0\frac{\partial}{\partial X} + V_1\frac{\partial}{\partial r} - \frac{\partial V_1}{\partial r} + \frac{\partial R_j}{\partial X}\frac{\partial U_0}{\partial r}\right] \\ & \times\left(\frac{D_0 \Lambda A_0^2}{Z_j}\right), \quad j = 1,2,\end{aligned} \tag{42}$$

where $\mp$ refers to evaluation at $j = 1,2$, respectively.

The system of equations in Eq. (39) is not self-adjoint and in order to determine the solvability condition the leading-order adjoint eigenvector $\boldsymbol{\psi}_0^\dagger$ is required. If $\mathscr{F}^\dagger$ is the adjoint operator and $\langle\cdot,\cdot\rangle$ defines a suitable inner product, then the following identity must be satisfied:

$$\langle \boldsymbol{\psi}_0^\dagger, \mathscr{F}\boldsymbol{\psi}_0\rangle = \langle \mathscr{F}^\dagger\boldsymbol{\psi}_0^\dagger, \boldsymbol{\psi}_0\rangle. \tag{43}$$

Taking $\boldsymbol{\psi}_0^\dagger = (Y_1, Y_2, Y_3, Y_4, Y_5)$ and using the inner product

$$\langle \mathbf{J}, \mathbf{K}\rangle = \int_{R_1}^{R_2}\sum_{n=1}^{5} J_n^* K_n r\,\mathrm{d}r, \tag{44}$$

where * denotes the complex conjugate, then the adjoint eigenvector is determined by solving

$$\mathscr{F}^\dagger\boldsymbol{\psi}_0^\dagger = 0, \tag{45}$$

subject to the boundary conditions

$$rD_0\left(\pm\frac{D_0\Lambda^2 Y_1^*}{\mathrm{i}\omega Z_j} - \frac{\partial Y_1^*}{\partial r}\right) + r\Gamma Y_4^* + \frac{r}{\gamma}\frac{\partial \hat{S}_0}{\partial r}Y_5^* = 0, \quad \text{at } r = R_j(X), \quad j = 1,2. \tag{46}$$

Owing to the form of the governing equations, analytical expressions can be found for the adjoint solution in terms of the eigenfunction $\boldsymbol{\psi}_0$. The adjoint operator and the adjoint solution are given in Appendix B. The solvability condition is then obtained from the relation

$$\langle \boldsymbol{\psi}_0^\dagger, \mathscr{F}\boldsymbol{\psi}_1 \rangle = \langle \mathscr{F}^\dagger \boldsymbol{\psi}_0^\dagger, \boldsymbol{\psi}_1 \rangle + \left[Y_1^* r D_0 \left(\frac{\partial A_1}{\partial r} + \mathscr{R}_1 \right) + A_1 \left(r\Gamma Y_4^* - r D_0 \frac{\partial Y_1^*}{\partial r} + \frac{Y_5^* r}{\gamma} \frac{\partial \hat{S}_0}{\partial r} \right) \right]_{R_1}^{R_2}. \quad (47)$$

By using the relations $\mathscr{F}\boldsymbol{\psi}_1 = \mathbf{f}$, $\mathscr{F}^\dagger \boldsymbol{\psi}_0^\dagger = 0$, and the boundary conditions in Eq. (42) to eliminate A_1 and $\mathscr{R}_1$, the solvability condition can be written in the form

$$\begin{aligned} \langle \boldsymbol{\psi}_0^\dagger, \mathbf{f} \rangle = {} & \left[R_2 D_0 A_0 \left\{ \frac{\partial R_2}{\partial X} \left(\mathrm{i}kA_0 + \mathscr{X}_0 + \frac{U_0 \hat{s}_0}{2} \right) - \frac{V_1 \hat{s}_0}{2} - \frac{\mathrm{i}}{A_0} \left\{ U_0 \frac{\partial}{\partial X} + V_1 \frac{\partial}{\partial r} - \frac{\partial V_1}{\partial r} \right.\right.\right. \\ & \left.\left.\left. + \frac{\partial R_2}{\partial X} \frac{\partial U_0}{\partial r} \right) \frac{D_0 \Lambda A_0^2}{\mathrm{i}\omega Z_2} \right\} \right]_{r=R_2} - \left[R_1 D_0 A_0 \left\{ \frac{\partial R_1}{\partial X} \left(\mathrm{i}kA_0 + \mathscr{X}_0 + \frac{U_0 \hat{s}_0}{2} \right) - \frac{V_1 \hat{s}_0}{2} \right.\right. \\ & \left.\left. + \frac{\mathrm{i}}{A_0} \left\{ U_0 \frac{\partial}{\partial X} + V_1 \frac{\partial}{\partial r} - \frac{\partial V_1}{\partial r} + \frac{\partial R_1}{\partial X} \frac{\partial U_0}{\partial r} \right) \frac{D_0 \Lambda A_0^2}{\mathrm{i}\omega Z_1} \right\} \right]_{r=R_1}. \end{aligned} \quad (48)$$

After some algebra the solvability condition can be rearranged to generate a governing equation for the amplitude function $N(X)$ of the form,

$$F(X) \frac{\mathrm{d}}{\mathrm{d}X} [N^2(X)] = G(X) N^2(X), \quad (49)$$

where expressions for $F(X)$ and $G(X)$ are given in Appendix B. The general solution is then

$$N^2(X) = N_0^2 \exp\left(\int^X \frac{G(\eta)}{F(\eta)} \mathrm{d}\eta \right), \quad (50)$$

where N_0 is a normalization constant.

Under the isentropic flow assumption ($\hat{S}_0 = 0$) the expressions for $F(X)$ and $G(X)$ reduce to those given in Ref. [1], and in the further limit of zero mean vorticity the solution becomes exactly that derived by Rienstra [5].

In the final governing equation (49) there is no explicit dependence on ε, and since both sides contain only single X-derivatives the equation is invariant under tranformation back to the physical variable x [5], i.e. x can be substituted for X in Eqs. (49) and (50). It is therefore convenient to consider axial variations in the example calculations in terms of the physical variable x rather than the slow variable X.

5. Results

The following duct shape is used as an example throughout:

$$R_1(x) = 0.5482 + 0.05 \tanh(2x - 2), \quad R_2(x) = 1.1518 - 0.05 \tanh(2x - 2). \quad (51)$$

The unsteady pressure is characterized by the axial wavenumber $k(x)$ and the cross-sectionally averaged potential amplitude

$$A(x) = \left[\int_{R_1}^{R_2} |A_0(x,r)|^2 r \, \mathrm{d}r\right]^{1/2}. \tag{52}$$

For a hard-walled duct the pressure-dominated family of eigenmodes consists of a finite number of propagating (cut-on) modes and an infinite discrete set of cut-off modes. Each eigenmode is associated with a radial order and the cut-on modes occur at the lowest radial orders. Only the first radial-order is considered here.

5.1. Comparison between isentropic and non-isentropic flows

In order to compare with the results obtained from the standard isentropic flow assumption the initial mean entropy distribution is chosen as a prescribed initial condition, together with the initial mean velocity. At the inlet ($x = 0$) the flow conditions are then given by

$$U_0(x=0,r) = U_i, \quad W_0(x=0,r) = \Omega r, \quad V(x=0,r) = 0, \quad \hat{S}_0(x=0,r) = -\ln(\alpha r^{\beta}), \tag{53}$$

where α and β are constants to be specified. The form chosen for the mean entropy enables comparison between isentropic (α arbitrary, $\beta = 0$) and non-isentropic (α, β arbitrary) flows to be established.

At the duct inlet the radial momentum equation and the first relation in Eq. (5) become

$$\frac{1}{D_0}\frac{\partial P_0}{\partial r} = \frac{W_0^2}{r} = \Omega^2 r, \quad P_0 = \frac{D_0^{\gamma}}{\gamma \alpha r^{\beta}}, \tag{54}$$

which can be used to determine an equation for the initial mean density

$$\frac{1}{(\gamma-1)}\frac{\partial (D_0^{\gamma-1})}{\partial r} - \frac{\beta}{\gamma r} D_0^{(\gamma-1)} = \alpha r^{\beta-1} W_0^2. \tag{55}$$

This has solution

$$D_0(X=0,r) = r^{\beta/\gamma}\left\{\frac{\alpha(\gamma-1)\Omega^2 r^{2+\beta/\gamma}}{2+\beta/\gamma} + K_3\right\}^{1/(\gamma-1)}, \tag{56}$$

where K_3 is an arbitrary constant chosen such that $D_0(x=0, R_1(0)) = 1$ when $\beta = 0, \alpha = 1$. Integration of the first term in Eq. (15) then gives

$$\psi(x=0,r) = \frac{U_i}{\gamma\alpha\Omega^2}\left[\frac{\alpha(\gamma-1)\Omega^2 r^{2+\beta/\gamma}}{2+\beta/\gamma} + 1\right]^{\gamma/(\gamma-1)} - K_4, \tag{57}$$

where the constant K_4 is chosen such that $\psi(x=0, R_1(0)) = 0$. The expression for the streamfunction is then rearranged to provide an expression for r in terms of ψ which is used to obtain expressions for H, C and $\mathscr{S}$ in terms of ψ alone. The coupled Eqs. (22) and (23), together with the boundary conditions, are then solved iteratively to determine the evolution of ψ and D_0 downstream.

The mean flow solutions for three different initial mean entropy distributions are shown in Fig. 1. The initial mean entropy profiles used are the isentropic case $\hat{S}_0 = 0$ given by $\beta = 0$, $\alpha = 1$,

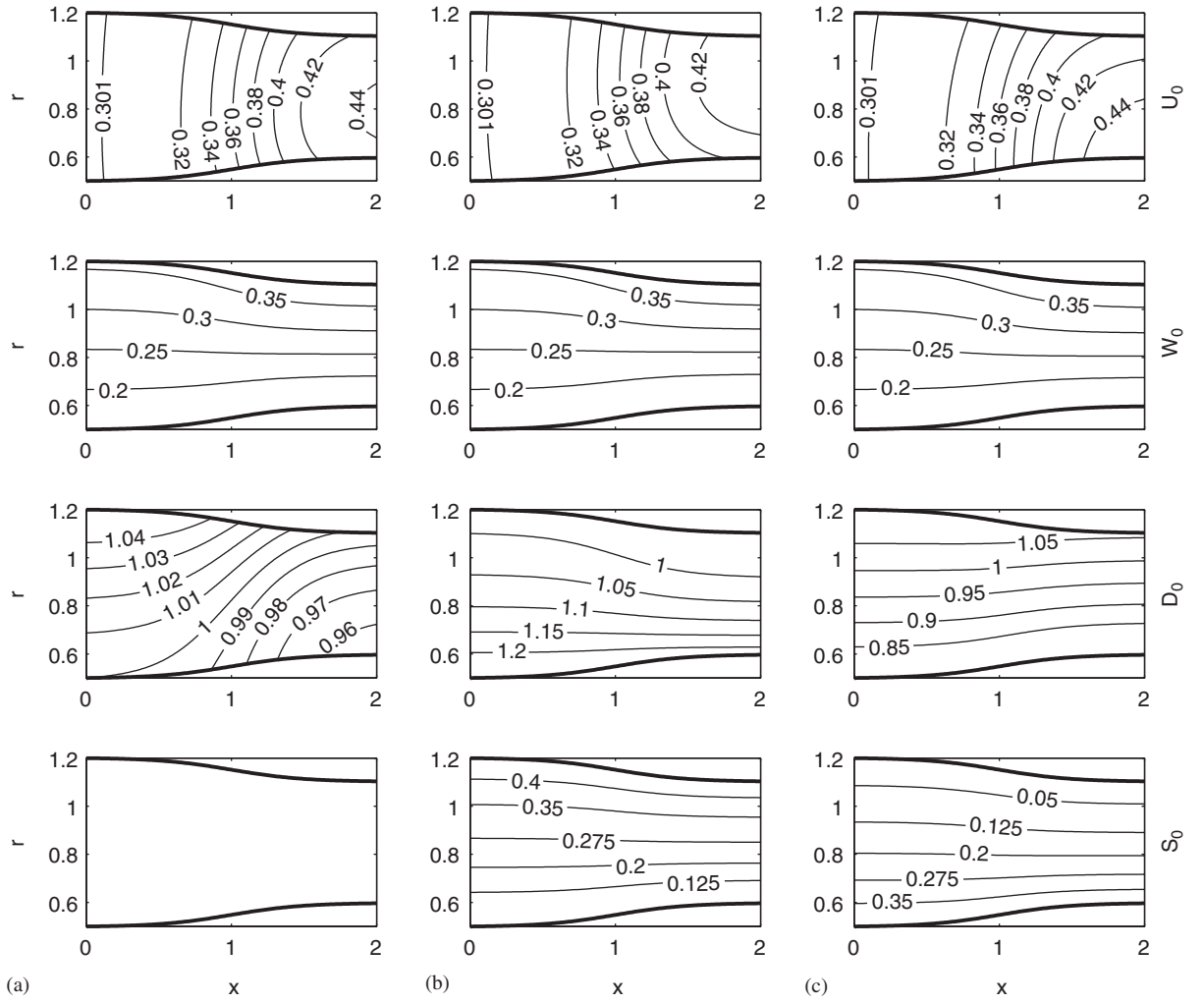

Fig. 1. Mean flow field generated by the inlet conditions $U_0(x=0,r)=0.3$, $W_0(x=0,r)=0.3r$, and the entropy distributions given by: (a) $\hat{S}_0=0$; (b) $\beta=-0.5$; (c) $\beta=0.5$. The first row shows the mean axial velocity U_0, the second row W_0, the third row D_0 and the fourth row $\hat{S}_0$.

the positive entropy gradient given by $\beta=-0.5$, $\alpha=R_1(0)^{-\beta}$, and the negative entropy gradient given by $\beta=0.5$, $\alpha=R_2(0)^{\beta}$. In each case $U_i=0.3$ and $\Omega=0.3$. Note that the initially uniform axial velocity develops some radial variation as it moves along the duct, and the radial profiles downstream depend on the form of the initial mean entropy profile. The main differences to the flow patterns resulting from the different initial entropy distributions occur in the form of the mean density. A very different initial profile is generated which affects the subsequent evolution, with much larger density variations observed for the non-isentropic ($\beta\neq 0$) cases.

The unsteady flow field is now determined for initial mean entropy distributions corresponding to two case of isentropic flow ($\hat{S}_0=0$ and 0.24) and two cases of mean entropy gradient specified by $\beta=\pm 0.5$. Results are presented for a hard-walled duct with $m=12$ and $\omega=18$. These initial entropy profiles give

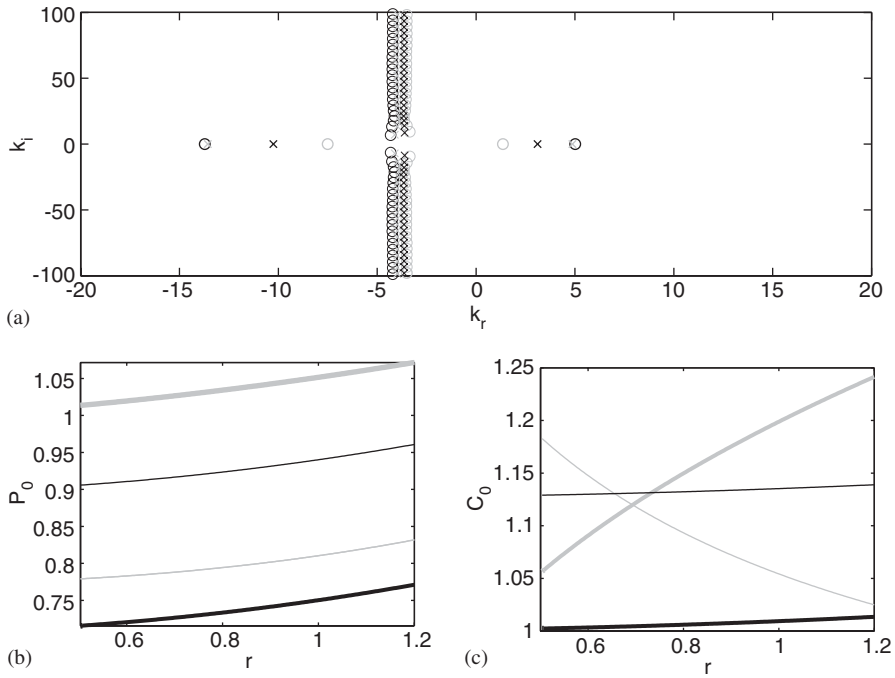

Fig. 2. (a) Initial acoustic eigenvalue spectra for the entropy distributions given by $\hat{S}_0 = 0$ (black circles), $\beta = 0.5$ (grey crosses), $\hat{S}_0 = 0.24$ (black crosses); (b) initial mean pressure distributions; (c) initial mean sound speed distributions. Bold black line: $\hat{S}_0 = 0$, thin grey line: $\beta = 0.5$, bold grey line: $\beta = -0.5$, thin black line: $\hat{S}_0 = 0.24$ ($m = 12, \omega = 18$).

rise to different initial distributions of the mean density (and mean pressure) as well as affecting the subsequent evolution. The changes to the initial conditions are reflected by differences in the initial eigenvalue spectra which are shown in Fig. 2(a). This shows that the $\hat{S}_0 = 0$ case has a cut-on mode furthest from cut-off, and the mode for the $\beta = -0.5$ case is closest to cut-off. This trend appears to be related to the relative levels of initial mean pressure (see Fig. 2(b)) where the highest/lowest levels of mean pressure correspond to the entropy distributions giving rise to modes closest to/furthest from cut-off. For isentropic flow the move toward cut-off with increasing mean entropy value can be attributed directly to increases in the mean sound speed (see Fig. 2(c)). Modes closest to cut-off exhibit the largest variation in amplitude (see Fig. 3) with significant differences observed between zero mean entropy flow and the positive entropy gradient flow. Similar trends are observed for all values of m, including negative values of m which correspond to modes counter-rotating to the mean swirl. Note that for isentropic flow the $O(1)$ energy equation (36) reduces to $\Lambda \hat{s}_0 = 0$. The purely convected solution, corresponding to $\Lambda = 0$, is not found but instead no entropic disturbance is generated ($\hat{s}_0 = 0$).

The effect of varying the initial mean entropy across a range of entropy gradients is now considered. The evolution of the axial wavenumbers for upstream and downstream-propagating modes in a hard-walled duct when $m = 12$, $\omega = 18$ is shown in Fig. 4(a) for initial mean entropy distributions given by $-0.6 \leqslant \beta \leqslant 0$ with the value of α chosen such that $\hat{S}_0 = 0$ at the inner radius. The effect of increasing the mean entropy gradient is to move the cut-on modes closer to cut-off. When the level of mean entropy is sufficiently high the upstream and downstream modes coalesce at some axial location and the modes become cut-off (see results for $\beta = -0.6$). The move toward

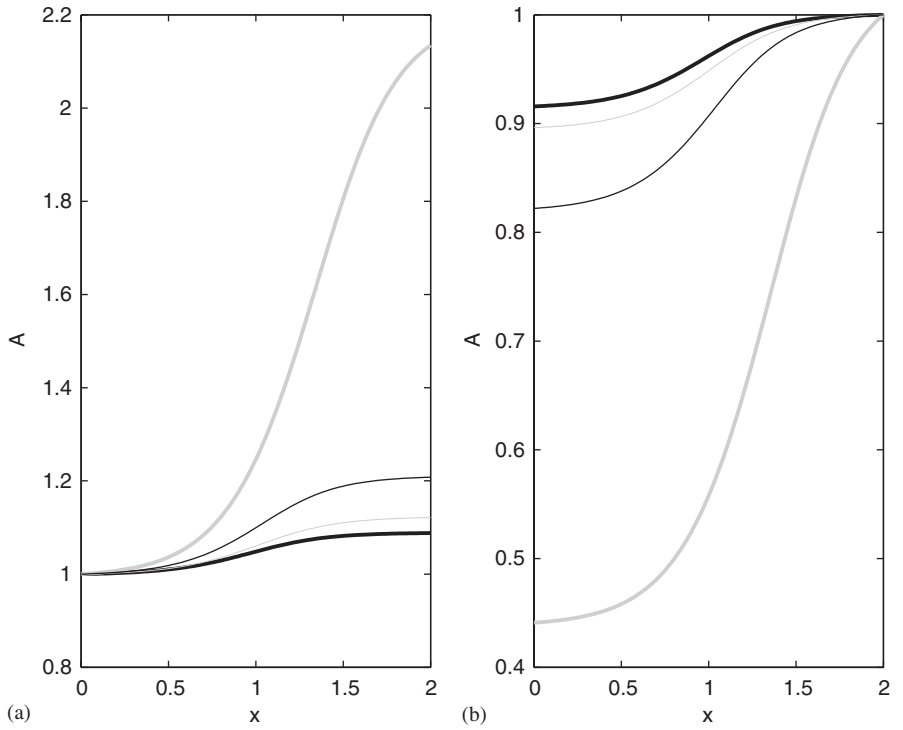

Fig. 3. Cross-sectionally averaged amplitudes for initial mean entropy profiles given by $\hat{S}_0 = 0$: bold black line; $\beta = 0.5$: thin grey line; $\beta = -0.5$: bold grey line; $\hat{S}_0 = 0.24$: thin black line: (a) downstream-propagating modes with amplitudes normalized to 1 at $x = 0$; (b) upstream-propagating modes with amplitudes normalized to 1 at $x = 2$.

cut off is reflected in the cross-sectionally averaged amplitudes shown in Figs. 4(b) and (c), where as $|\beta|$ increases (and the modes become closer to cut-off), the amplitude undergoes significant variation along the duct. If β is taken to be positive, with α chosen such that $\hat{S}_0 = 0$ at the outer radius, then there is still a trend toward cut-off as β increases, but the effect is much smaller as demonstrated in Fig. 5.

The general effect of varying the initial mean entropy gradient and the influence of frequency is assessed by plotting the cross sectionally averaged amplitude at the duct end points as a function of β. This is shown in Fig. 6 for $m = 12$ and the frequency values $\omega = 16$–18. Also shown are the corresponding results for the equivalent isentropic case, where the value of the uniform mean entropy is chosen to be the mean value of the entropy gradient given by

$$\text{mean}(\hat{S}_0) = \frac{2}{R_2^2(0) - R_1^2(0)} \int_{R_1(0)}^{R_2(0)} -\ln(\alpha r^{\beta}) r \, \mathrm{d}r. \tag{58}$$

This attempts to identify whether the variation from the $\hat{S}_0 = 0$ ($\alpha = 1, \beta = 0$) case occurs as a result of the increase in value of the entropy or as a result of the entropy gradient. Negative values of β (positive entropy gradient) always push the modes furthest toward cut-off resulting in strong amplitude variation. For positive values of β (negative entropy gradient) the trend is also toward cut-off but the amplitude variation is less than that for the corresponding mean isentropic

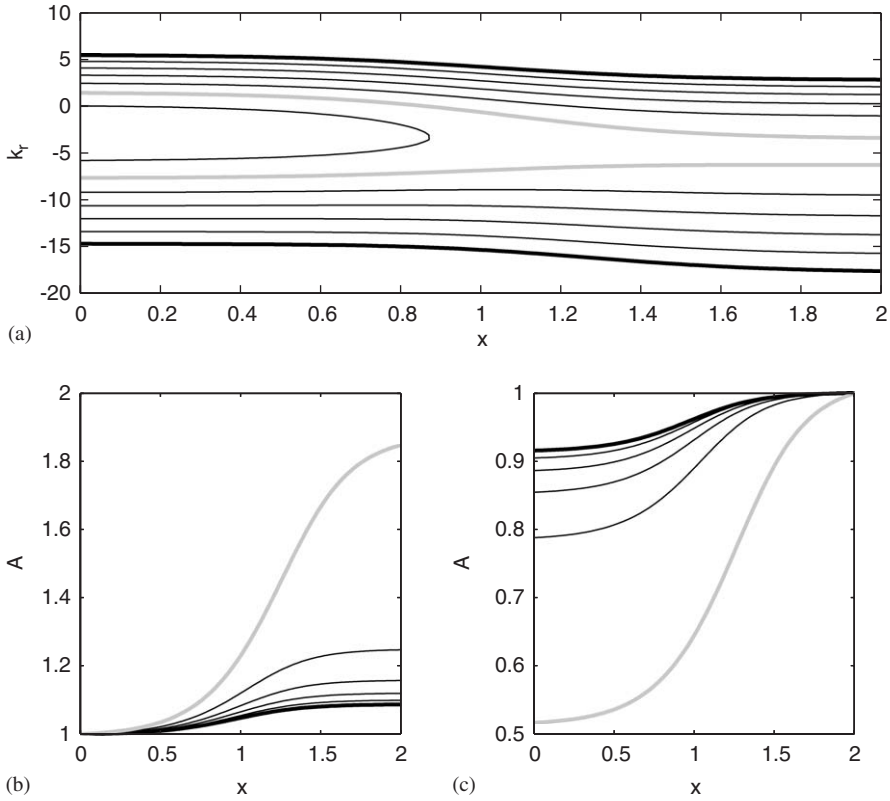

Fig. 4. (a) Evolution of axial wavenumber $k(x)$ with values of $\beta = -0.6$ to 0, in steps of 0.1. Bold black lines are for $\beta = 0$, bold grey lines are for $\beta = -0.5$. Upper/lower lines correspond to downstream/upstream-propagating modes. For $\beta < -0.5$ the mode becomes cut-off ($k_i \neq 0$) at some point along the duct. (b) Variation in cross-sectionally averaged amplitude for downstream-propagating modes. (c) Variation in cross-sectionally averaged amplitude for upstream-propagating modes.

value. The positive/negative mean entropy gradient appears to enhance/diminish the effect brought about by non-zero uniform mean entropy. Fig. 6 also demonstrates the trend brought about by frequency variation. For a given level of mean entropy amplitudes at the duct end points increase as modes become closer to cut-off. The strong variation with frequency in Fig. 6 can be explained by the fact that as the frequency increases modes move further away from cut-off. This effect is enhanced as the entropy gradient increases. For each frequency the mode produced when $\hat{S}_0 = 0$ is the most cut-on and exhibits the least amplitude variation.

5.2. Uniform initial density, effect of swirl

In order to determine how the mean swirl affects the entropy distribution the following conditions are now applied as the initial mean field at the duct inlet:

$$U_0(x = 0, r) = U_i, \quad W_0(x = 0, r) = \Omega r + \Upsilon/r, \quad V(x = 0, r) = 0, \quad D_0(x = 0, r) = 1. \tag{59}$$

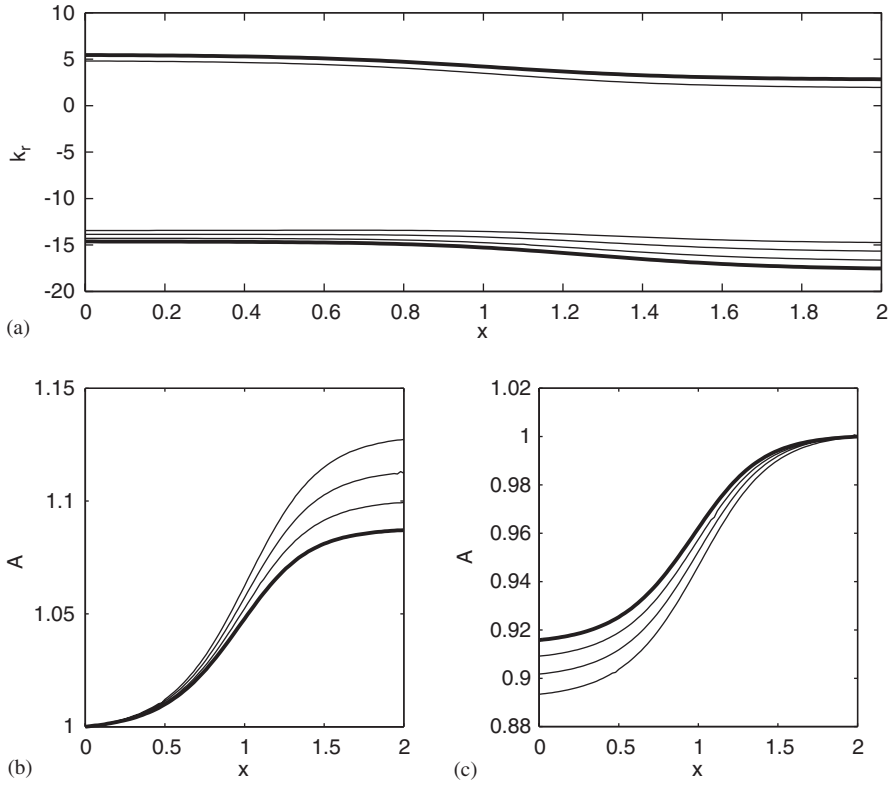

Fig. 5. (a) Evolution of axial wavenumber $k(x)$ with values of $\beta = 0$ to 0.6 in steps of 0.2. Bold black lines are for $\beta = 0$. Upper lines correspond to downstream-propagating modes (only lines for $\beta = 0$ and 0.6 are shown). Lower lines correspond to downstream/upstream-propagating modes. (b) Variation in cross-sectionally averaged amplitude for downstream-propagating modes. (c) Variation in cross-sectionally averaged amplitude for upstream-propagating modes.

The radial momentum equation defines the initial mean pressure as

$$P_0(x=0,r) = \frac{\Omega^2}{2}(r^2 - r_1^2) + 2\Omega\Upsilon \ln\left(\frac{r}{r_1}\right) + \frac{\Upsilon^2}{2}\left(\frac{r^2 - r_1^2}{r^2 r_1^2}\right) + \frac{1}{\gamma}, \tag{60}$$

where $r_1 = R_1(0)$. The initial mean entropy is then determined from $S_0/c_v = \ln(\gamma P_0)$. Integration of the first expression in Eq. (15) with respect to r determines the streamfunction as

$$\psi(x=0,r) = \frac{U_i}{2}(r^2 - r_1^2), \tag{61}$$

which can again be rearranged to express r in terms of ψ, and used subsequently to obtain analytical expressions for H, C and $\mathscr{S}$ in terms of ψ alone. The mean field for $U_i = 0.3$, $\Omega = 0.3$ and $\Upsilon = 0.2$ generates a mean entropy distribution with positive gradient as shown in Fig. 7. If the initial mean swirl is increased then this results in an increase in the level of mean entropy as shown in Fig. 8. It is also evident that the rigid-body component of the mean swirl increases and the free-vortex component decreases as x increases.

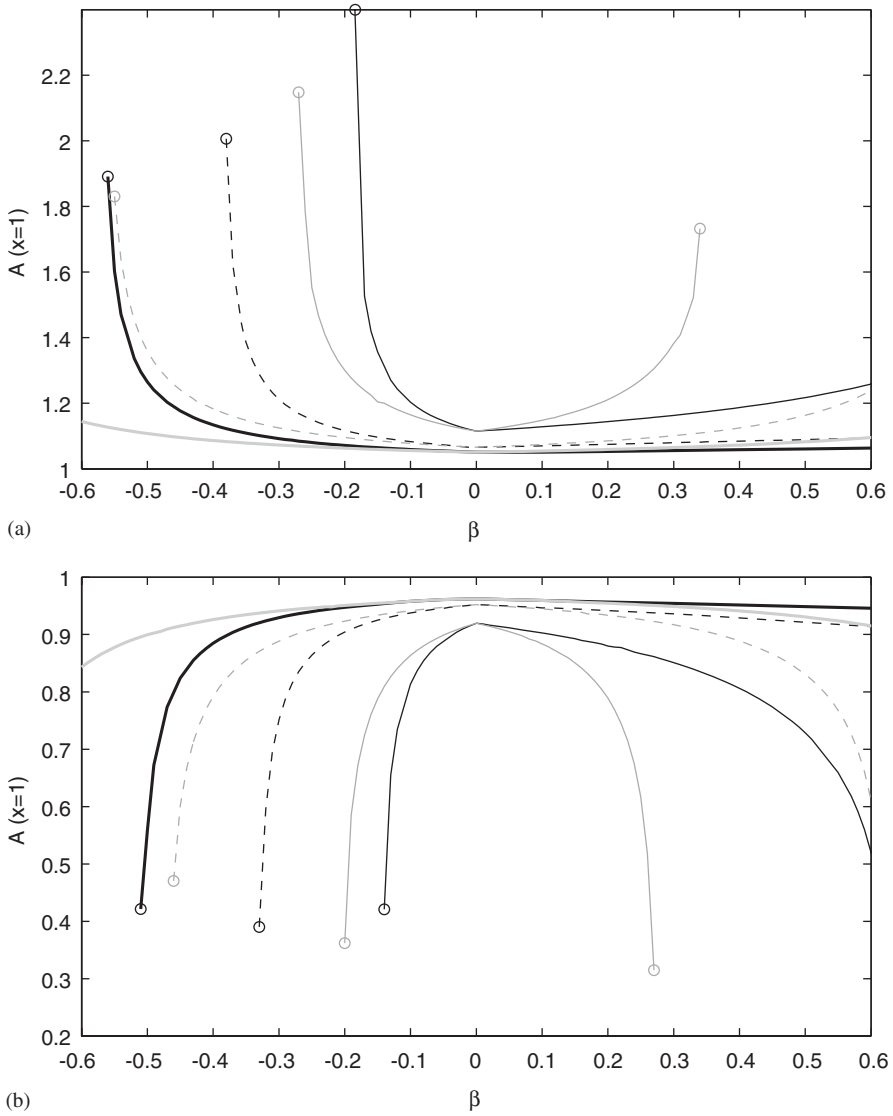

Fig. 6. Variation in cross-sectionally averaged amplitude at $x = 1$ with initial mean entropy profile: (a) downstream-propagating modes; (b) upstream-propagating modes. Bold black line: $\omega = 18$, dashed black line : $\omega = 17$, thin black line: $\omega = 16$. Grey lines are the corresponding results for uniform mean entropy. Circles denote where the mode becomes cut-off ($m = 12$).

Swirl is known to cut-off co-rotating modes ($m > 0$) which are cut-on in the absence of swirl [18]. For modes which are counter-rotating ($m < 0$) the effect of swirl is to cut-on modes. The effect of the different levels of initial mean swirl on the unsteady field is shown in Fig. 9. This shows that the trend toward cut-off with increasing swirl is also observed when non-uniform mean entropy is included. The effect of placing an acoustic lining on the outer wall is shown in Fig. 10. The downstream/upstream-propagating cut-on modes are pushed into the upper/lower halves of

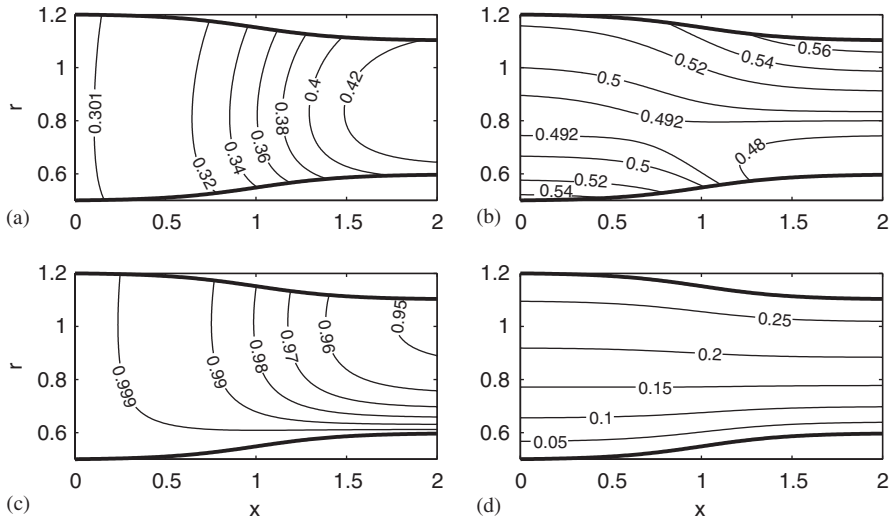

Fig. 7. Mean flow field generated by the inlet conditions $U_0(x=0,r)=0.3$, $W_0(x=0,r)=0.3r+0.2/r$, $D_0(x=0,r)=1$: (a) U_0; (b) W_0; (c) D_0; (d) $\hat{S}_0$.

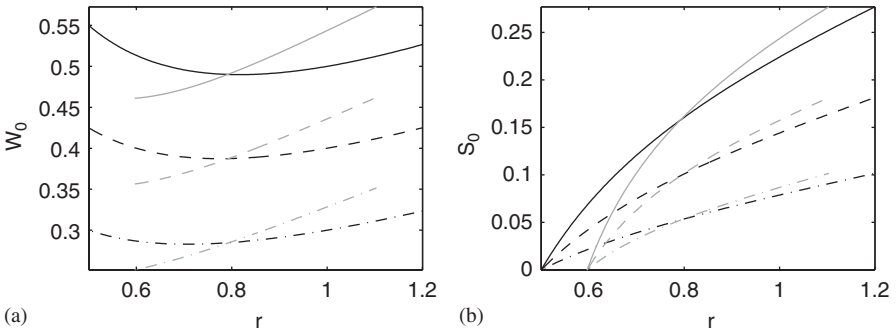

Fig. 8. Effect of different levels of initial mean swirl: (a) mean swirl distribution W_0; (b) mean entropy distribution $\hat{S}_0$. Solid lines: $\Omega=0.3$, $\Upsilon=0.2$, dashed lines: $\Omega=0.25$, $\Upsilon=0.15$, dash–dot lines: $\Omega=0.2$, $\Upsilon=0.1$. Black lines correspond to the profiles at $x=0$, the grey lines at $x=2$.

the complex k-plane. In order to interpret how damped the modes become account must be taken of both the variation of A and the exponential factor $\exp[i\int^x(k(\eta)/\varepsilon)\,\mathrm{d}\eta]$. This is accomplished by considering the function

$$B(x)=A(x)\exp\left(-\frac{1}{\varepsilon}\int^x k_i(\eta)\,\mathrm{d}\eta\right). \tag{62}$$

Fig. 10(c) shows that the upstream-propagating modes are the most damped owing to larger values of $|k_i|$. The acoustic lining is most effective for modes which are closest to cut-off in a hard-walled duct.

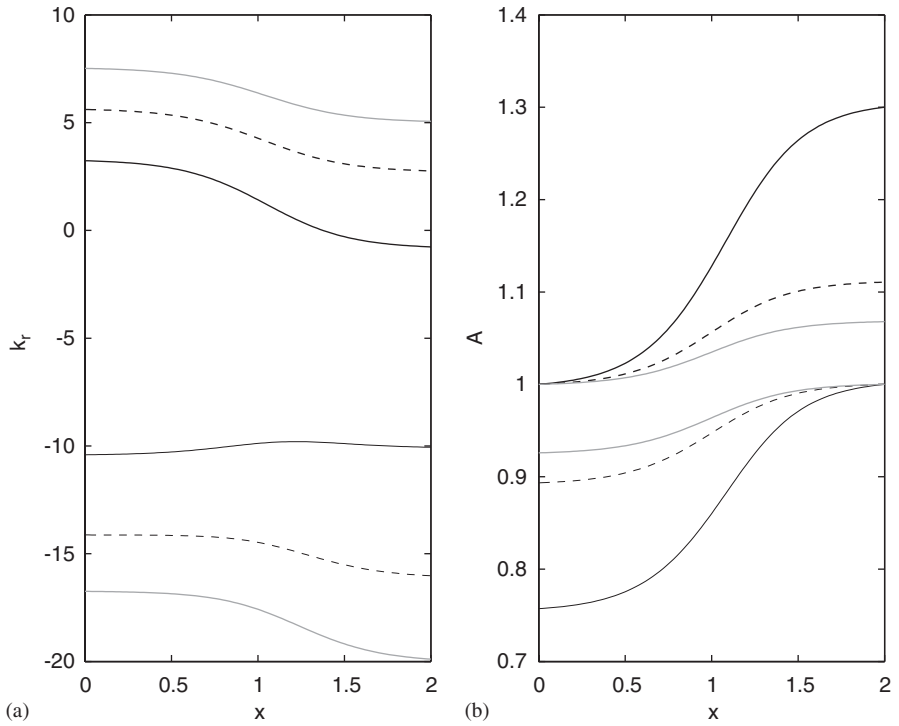

Fig. 9. (a) Evolution of axial wavenumber $k(x)$ for different levels of initial mean swirl; (b) corresponding cross-sectionally averaged amplitudes. Black solid line: $\Omega = 0.3$, $\Upsilon = 0.2$, black dashed line: $\Omega = 0.25$, $\Upsilon = 0.15$, grey solid line: $\Omega = 0.2$, $\Upsilon = 0.1$ ($m = 12, \omega = 20$).

5.3. Turning-point solution

The general multiple-scales solution in Eq. (50) breaks down when $F(X) = 0$, and this occurs at the transition from cut-on to cut-off at so-called turning points. The cut-on cut-off transition is found in many flow cases including both swirling and irrotational flows. Here, and for isentropic swirling flow, F^2 passes through zero at the turning point, so that on one side of the turning point F is real and on the other side F is complex. A non-singular solution for the isentropic case was derived in Ref. [1] by including higher-order second derivatives in the solvability condition. The amplitude in the region of the turning point is then governed by a form of Airy's equation. The same process can be carried out for non-isentropic flow and it is found that the inclusion of non-zero mean entropy does not change the general structure of the solution in the turning-point region.

6. Concluding remarks

This paper describes how a systematic approximate solution is constructed for sound propagation through varying ducts with a mean flow that contains swirl and non-uniform entropy. Within this analysis a systematic mean flow solution for the slowly-varying duct is

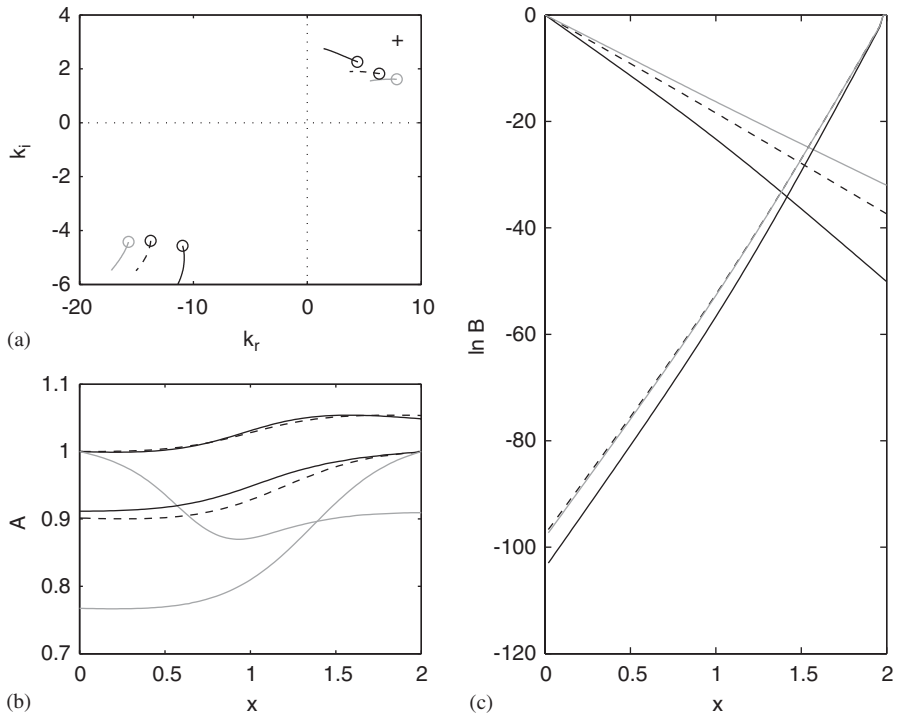

Fig. 10. Effect of acoustic lining on outer wall: (a) axial wavenumber in complex plane—circles denote the value at $x = 0$; (b) cross-sectionally averaged amplitudes; (c) values of $\ln B$. Line types correspond to those in Fig. 9 ($m = 12, \omega = 20, Z_2 = 2 - \mathrm{i}, \varepsilon = 0.1$).

determined. It is shown that the propagation of acoustic modes can be affected strongly by non-uniform mean entropy. Even in the case of a uniform duct the differences between assuming isentropic and non-isentropic flows can be significant, particularly in the cut-on cut-off nature of the acoustic modes. Any form of non-zero mean entropy is found to push modes toward cut-off.

Positive entropy gradients are found to have the most effect on the propagation of acoustic modes, producing modes much closer to cut-off. Negative mean entropy gradients are found to have less effect than the corresponding mean isentropic value. The slow axial variation in the duct enhances the changes to the cut-on/cut-off nature of the duct modes since those modes which are closest to cut-off exhibit much larger variations in amplitude. The importance of accounting for the mean entropy distribution is therefore of two-fold importance. Since only cut-on modes contribute to the generated noise field, the cut-on/cut-off nature of the modes affects the propagation of noise along the duct. Suppose, under the standard isentropic flow assumption, a mode is cut-on. If the mean entropy distribution is accounted for then this mode may still be cut-on but undergo significantly different amplitude variation which would, in turn, affect the level of noise. Alternatively the mode may actually become cut-off and therefore no longer contribute to the noise field.

It has also been shown that as the level of mean swirl increases the mean entropy increases. It is therefore essential that mean entropy variations be accounted for in strongly swirling flows. The

effect of acoustic lining is also included in the analysis and results show that the liner is generally most effective for modes closest to cut-off. Again, due to the effect of mean entropy on the cut-on/cut-off behaviour of the modes this would have implications for the effectiveness of acoustic linings.

Acknowledgements

This work was supported by The Royal Society. The author is also grateful to Prof. N. Peake for helpful discussions.

Appendix A

The operators $\mathscr{L}$ and $\mathscr{K}$ defining the linear eigenvalue problem in Eq. (39) are

$$\mathscr{L} = \begin{bmatrix} \mathscr{P} & \left(-\dfrac{2U_0\omega_m D_0}{C_0^2\beta_0^2}\right) & \left(D_0\dfrac{\partial}{\partial r}+\dfrac{1}{r}\dfrac{\partial rD_0}{\partial r}\right) & \dfrac{D_0 m}{r} & \left(\dfrac{\omega}{2}+\dfrac{\omega_m}{2}\right)D_0 \\ 0 & \dfrac{1}{\beta_0^2} & 0 & 0 & 0 \\ -\dfrac{m\Gamma}{r}-\dfrac{\omega_m}{\gamma}\dfrac{\partial\hat{S}_0}{\partial r} & 0 & -\omega_m & \dfrac{2W_0}{r} & 0 \\ \Gamma\dfrac{\partial}{\partial r} & 0 & \Gamma & -\omega_m & -\dfrac{\omega_m W_0}{2} \\ \dfrac{1}{\gamma}\dfrac{\partial\hat{S}_0}{\partial r}\dfrac{\partial}{\partial r} & 0 & \dfrac{1}{\gamma}\dfrac{\partial\hat{S}_0}{\partial r} & 0 & -\omega_m \end{bmatrix},$$

$$\mathscr{K} = \begin{bmatrix} 0 & D_0 & 0 & -\dfrac{\partial U_0}{\partial r}\dfrac{D_0}{\Gamma} & \left(U_0 D_0 - \dfrac{D_0}{2\Gamma}\dfrac{\partial U_0}{\partial r}W_0\right) \\ 1 & 0 & 0 & 0 & 0 \\ \dfrac{\partial U_0}{\partial r}-\dfrac{U_0}{\gamma}\dfrac{\partial\hat{S}_0}{\partial r} & 0 & -U_0 & 0 & 0 \\ 0 & 0 & 0 & -U_0 & -\dfrac{U_0 W_0}{2} \\ 0 & 0 & 0 & 0 & -U_0 \end{bmatrix},$$

where $\omega_m = \omega - mW_0/r$ and $\mathscr{P}$ is the operator

$$\mathscr{P} = \frac{1}{r}\frac{\partial}{\partial r}\left(rD_0\frac{\partial}{\partial r}\right) + D_0\left(\frac{\omega_m^2}{C_0^2}-\frac{m^2}{r^2}\right).$$

Appendix B

The vector $\mathbf{f}$ appearing on the right-hand-side of the $O(\varepsilon)$ linear eigenvalue problem (41) takes the form $\mathbf{f} = (f_A, f_\eta, f_{\mathscr{R}}, f_{\mathscr{T}}, f_s)$ where

$$f_A = \mathrm{i}\left\{\frac{1}{A_0}\frac{\partial}{\partial X}\left[\left(\frac{U_0\Lambda}{C_0^2} - k\right)D_0A_0^2\right] + \frac{1}{rA_0}\frac{\partial}{\partial r}\left[\frac{r\Lambda V_1}{C_0^2}D_0A_0^2\right] + \frac{\partial}{\partial X}(\mathrm{i}D_0\mathscr{X}_0) - \frac{\partial}{\partial X}(U_0D_0\mathrm{i}\hat{s}_0) - \frac{1}{r}\frac{\partial}{\partial r}(rV_1D_0\mathrm{i}\hat{s}_0) - \frac{kD_0}{\mathrm{i}\Lambda\Gamma}\left(\Gamma f_{\mathscr{X}} - \frac{\partial U_0}{\partial r}f_{\mathscr{T}}\right)\right\}, \tag{63}$$

$$f_\eta = 0, \tag{64}$$

$$f_{\mathscr{R}} = \mathrm{i}\left\{U_0\frac{\partial\mathscr{R}_0}{\partial X} - \frac{\partial U_0}{\partial r}\frac{\partial A_0}{\partial X} + V_1\frac{\partial\mathscr{R}_0}{\partial r} + \mathscr{R}_0\frac{\partial V_1}{\partial r} + \frac{1}{\gamma}\frac{\partial\hat{S}_0}{\partial r}\left(U_0\frac{\partial A_0}{\partial X} + V_1\frac{\partial A_0}{\partial r}\right) + \frac{\mathrm{i}\Lambda V_1\hat{s}_0}{2}\right\}, \tag{65}$$

$$f_{\mathscr{T}} = -V_1\frac{\partial\mathscr{T}_0}{\partial r} - U_0\frac{\partial\mathscr{T}_0}{\partial X} - \frac{V_1}{r}\mathscr{T}_0 - \frac{\partial W_0}{\partial X}\mathscr{X}_0 - \frac{\partial W_0}{\partial X}\mathrm{i}kA_0 - \frac{W_0}{2}\left(U_0\frac{\partial\hat{s}_0}{\partial X} + V_1\frac{\partial\hat{s}_0}{\partial r}\right), \tag{66}$$

$$f_s = -V_1\frac{\partial\hat{s}_0}{\partial r} - U_0\frac{\partial\hat{s}_0}{\partial X} - \frac{V_1}{2\gamma}\hat{s}_0\frac{\partial\hat{S}_0}{\partial r} - \frac{1}{\gamma}\frac{\partial\hat{S}_0}{\partial X}\left(\mathrm{i}kA_0 + \mathscr{X}_0 + \frac{U_0}{2}\hat{s}_0\right), \tag{67}$$

where

$$f_{\mathscr{X}} = -V_1\frac{\partial\mathscr{X}_0}{\partial r} - U_0\frac{\partial\mathscr{X}_0}{\partial X} - \frac{\partial U_0}{\partial X}\mathscr{X}_0 + \frac{\partial W_0}{\partial X}\frac{\mathrm{i}mA_0}{r} - \frac{\mathrm{i}\Lambda A_0}{\gamma}\frac{\partial\hat{S}_0}{\partial X} - \frac{U_0}{2}\left(U_0\frac{\partial\hat{s}_0}{\partial X} + V_1\frac{\partial\hat{s}_0}{\partial r}\right). \tag{68}$$

The adjoint operator $\mathscr{F}^\dagger$ is

$$\mathscr{F}^\dagger = \begin{bmatrix} \mathscr{P} & -k^* & -\dfrac{m\Gamma}{r} - k^*\dfrac{\partial U_0}{\partial r} + \left(\dfrac{k^*U_0}{\gamma} - \dfrac{\omega_m}{\gamma}\right)\dfrac{\partial\hat{S}_0}{\partial r} \\ -D_0\left(\dfrac{2U_0\omega_m}{C_0^2\beta_0^2} + K^*\right) & \dfrac{1}{\beta_0^2} & 0 \\ -D_0\dfrac{\partial}{\partial r} & 0 & k^*U_0 - \omega_m \\ D_0\left(\dfrac{m}{r} + \dfrac{k^*\partial U_0/\partial r}{\Gamma}\right) & 0 & \dfrac{2W_0}{r} \\ D_0\left(\dfrac{\omega}{2} + \dfrac{\omega_m}{2} - k^*U_0 + \dfrac{k^*\partial U_0/\partial r W_0}{2\Gamma}\right) & 0 & 0 \end{bmatrix}$$

$$\begin{bmatrix} -\Gamma\dfrac{\partial}{\partial r}-\dfrac{1}{r}\dfrac{\partial(r\Gamma)}{\partial r} & -\dfrac{1}{\gamma}\dfrac{\partial\hat{S}_0}{\partial r}\dfrac{\partial}{\partial r}-\dfrac{1}{r}\dfrac{\partial}{\partial r}\left(\dfrac{r}{\gamma}\dfrac{\partial\hat{S}_0}{\partial r}\right) \\ 0 & 0 \\ \Gamma & \dfrac{1}{\gamma}\dfrac{\partial\hat{S}_0}{\partial r} \\ k^*U_0-\omega_m & 0 \\ (k^*U_0-\omega_m)\dfrac{W_0}{2} & k^*U_0-\omega_m \end{bmatrix}.$$

The adjoint solution is

$$Y_1 = A_0^*, \tag{69}$$

$$Y_2 = \left(\frac{2\omega_m U_0}{C_0^*\beta_0^2}+k^*\right)D_0\beta_0^2A_0^*, \tag{70}$$

$$Y_3 = \frac{\mathrm{i}D_0\mathscr{T}_0^*}{\Gamma}-\frac{D_0\Lambda^* r}{\Gamma 2W_0\gamma}\frac{\partial\hat{S}_0}{\partial r}\left(A_0^*-\frac{Y_5}{D_0}\right), \tag{71}$$

$$Y_4 = -\frac{D_0\mathscr{R}_0^*}{\Gamma}-\frac{1}{\Gamma\gamma}\frac{\partial\hat{S}_0}{\partial r}Y_5, \tag{72}$$

$$Y_5 = D_0A_0^*+\frac{\mathrm{i}D_0W_0^2\gamma}{r\partial\hat{S}_0/\partial r}\hat{s}_0^*. \tag{73}$$

The functions appearing in Eq. (49) are

$$F(X) = \int_{R_1}^{R_2}\left\{\frac{r\omega\sigma}{C_0}D_0A_0^2+\frac{A_0rD_0}{2}(\mathrm{i}\mathscr{X}_0-U_0\mathrm{i}\hat{s}_0)+\frac{r}{2}Y_3^*\left(U_0\mathscr{R}_0-\frac{\partial U_0}{\partial r}A_0+\frac{1}{\gamma}\frac{\partial\hat{S}_0}{\partial r}U_0A_0\right)\right.$$
$$\left.+\frac{rY_4^*}{2}\left(U_0\mathrm{i}\mathscr{T}_0+\frac{U_0W_0}{2}\mathrm{i}\hat{s}_0\right)+\frac{rY_5^*}{2}U_0\mathrm{i}\hat{s}_0\right\}\mathrm{d}r-\left[\frac{rD_0U_0D_0\Lambda A_0^2}{\mathrm{i}\omega Z_2}\right]_{R_2}-\left[\frac{rD_0U_0D_0\Lambda A_0^2}{\mathrm{i}\omega Z_1}\right]_{R_1},$$

$$G(X) = -\int_{R_1}^{R_2}\left\{\frac{\partial}{\partial X}\left(\frac{r\omega\sigma}{C_0}D_0A_0^2\right)+rD_0\frac{\partial}{\partial X}(\mathrm{i}D_0\mathscr{X}_0)-rA_0\frac{\partial}{\partial X}(U_0D_0\mathrm{i}\hat{s}_0)+\frac{\partial}{\partial r}\left(\frac{r\Lambda V_1}{C_0^2}D_0A_0^2\right)\right.$$
$$\left.-A_0\frac{\partial}{\partial r}(rV_1D_0\mathrm{i}\hat{s}_0)-\mathrm{i}rY_3^*f_{\mathscr{R}}-\mathrm{i}rY_4^*f_{\mathscr{T}}-rY_5^*f_s-\frac{\mathrm{i}rA_0kD_0}{\Lambda\Gamma}\left(\Gamma f_{\mathscr{X}}-\frac{\partial U}{\partial r}f_{\mathscr{R}}\right)\right\}\mathrm{d}r$$
$$+\left[A_0rD_0\left\{-\frac{\partial R_j}{\partial X}\left(\mathrm{i}\mathscr{X}_0-kA_0+\frac{U_0\mathrm{i}\hat{s}_0}{2}\right)+\frac{V_1\mathrm{i}\hat{s}_0}{2}\mp rD_0\left\{U_0\frac{\partial}{\partial X}+V_1\frac{\partial}{\partial r}\right.\right.\right.$$
$$\left.\left.\left.-\frac{\partial V_1}{\partial r}+\frac{\partial R_j}{\partial X}\frac{\partial U_0}{\partial r}\right\}\frac{D_0\Lambda A_0^2}{\mathrm{i}\omega Z_j}\right\}\right]_{R_1}^{R_2},$$

where $\mp$ refers to evaluation at R_1 and R_2, respectively, and

$$\frac{\omega\sigma}{C_0} = \frac{U_0 \Lambda}{C_0^2} + k.$$

References

[1] A.J. Cooper, N. Peake, Propagation of unsteady disturbances in a slowly varying duct with mean swirling flow, *Journal of Fluid Mechanics* 445 (2001) 207–234.

[2] A.H. Nayfeh, J.E. Kaiser, D.P. Telionis, Transmission of sound through annular ducts of varying cross sections, *AIAA Journal* 13 (1975) 60–65.

[3] A.H. Nayfeh, B.S. Shaker, J.E. Kaiser, Transmission of sound through nonuniform circular ducts with compressible mean flow, *AIAA Journal* 18 (1980) 515–525.

[4] A.H. Nayfeh, D.P. Telionis, Acoustic propagation in ducts with varying cross-sections, *Journal of the Acoustical Society of America* 54 (1973) 1654–1661.

[5] S.W. Rienstra, Sound transmission through lined ducts with flow, *Journal of Fluid Mechanics* 380 (1999) 279–296.

[6] S.W. Rienstra, W. Eversman, A numerical comparison between multiple-scales and finite-element solutions for sound propagation in lined flow ducts, *Journal of Fluid Mechanics* 437 (2001) 367–384.

[7] N. Peake, A.J. Cooper, Acoustic propagation in ducts with slowly varying elliptic cross section, *Journal of Sound and Vibration* 243 (2001) 381–401.

[8] S.W. Rienstra, Sound propagation in slowly varying lined ducts of arbitrary cross section, *Journal of Fluid Mechanics* 495 (2003) 157–173.

[9] V.V. Golubev, H.M. Atassi, Acoustic-vorticity waves in swirling flows, *Journal of Sound and Vibration* 209 (1998) 203–222.

[10] V.V. Golubev, H.M. Atassi, Unsteady swirling flows in annular cascades, Part 1: evolution of incident disturbances, *AIAA Journal* 38 (2000) 1142–1149.

[11] C.K.W. Tam, L. Auriault, The wave modes in ducted swirling flows, *Journal of Fluid Mechanics* 371 (1998) 1–20.

[12] S.Z. Shuja, B.S. Yilbas, A laminar swirling jet impingement onto an adiabatic wall—effect of inlet velocity profiles, *International Journal of Numerical Methods for Heat and Fluid Flow* 11 (2001) 237–254.

[13] S.Z. Shuja, B.S. Yilbas, M. Rashid, Confined swirling jet impingement onto an adiabatic wall, *International Journal of Heat and Mass Transfer* 46 (2003) 2947–2955.

[14] G.K. Bachelor, *An Introduction to Fluid Dynamics*, Cambridge University Press, Cambridge, 1967.

[15] M.E. Goldstein, Unsteady vortical and entropic disturbances of potential flows round arbitrary obstacles, *Journal of Fluid Mechanics* 89 (1978) 433–468.

[16] M.K. Myers, On the acoustic boundary condition in the presence of flow, *Journal of Sound and Vibration* 71 (1980) 429–434.

[17] M.R. Khorrami, A Chebyshev spectral collocation method using a staggered grid for the stability of cylindrical flows, *International Journal for Numerical Methods in Fluids* 12 (1991) 825–833.

[18] A.J. Cooper, N. Peake, Trapped acoustic modes in aeroengine intakes with swirling flow, *Journal of Fluid Mechanics* 419 (2000) 381–401.